Crystal dynamics of zinc chalcogenides I: an application to ZnS

Jay Prakash DUBEY[1],*, Raj Kishore TIWARI[2], Kripa Shankar UPADHYAYA[3], Pramod Kumar PANDEY[1]

[1]Department of Physics, Pandit Sambhoo Nath Shukla Government Post Graduate College, Affiliated to Awadhesh Pratap Singh University, Rewa, Madhya Pradesh, India
[2]Department of Physics, Government New Science College, Affiliated to Awadhesh Pratap Singh University, Rewa, Madhya Pradesh, India
[3]Department of Physics, Nehru Gram Bharati University, Allahabad, Uttar Pradesh, India

Abstract: A van der Waals three body force rigid shell model (VTRSM) developed earlier for NaCl and CsCl structure was expanded by us for zinc blende structure (ZBS). This model includes the effect of three body interactions and van der Waals interactions in the rigid shell model where short-range interactions were considered up to the second neighbor. Our model thus developed was applied to study the phonon dispersion curves, Debye temperature variation, two phonon Raman/IR spectra, and anharmonic elastic properties of ZnS. Our results are in good agreement with the measured data wherever available.

Key words: Phonons, van der Waals interactions, Debye temperature, combined density of states curve, Raman spectra, zinc sulfide, phonon dispersion curves, lattice dynamics

PACS: 63.20.-e, 65.40.Ba, 78.30.-j

1. Introduction

In recent years, there has been considerable interest in the theoretical and experimental studies of $A^N B^{8-N}$ type crystals of zinc blende structure (ZBS). This particular attention is primarily due to their high symmetry and simplicity of their ionic bonding. These semiconductor crystals are ZnS, ZnSe, ZnTe, GaP, GaSb, GaAs, InP, InAs, InSb etc. i.e. III–V and IIB–VIA groups of compounds. In this structure, ZnS, ZnSe, and ZnTe have wide band gaps and constitute a family of cubic crystal at ambient pressure. They have the remarkable property of transverse acoustic (TA) vibrations and have a large region at very low group velocity. The difference between frequencies of the longitudinal and transverse vibrations at the boundary of the Brillouin zone is very large. In this communication, we are mainly concerned with the crystal dynamics of zinc sulfide (ZnS). The experimental data on ZnS for phonon dispersion curves [1], harmonic and anharmonic elastic constants [2], Debye temperature variation [3,4], two phonon IR [5], and Raman spectra [6] are available. Further, there are different lattice dynamical models that have been used to explain the vibrational properties of these crystals. Amongst them are the rigid ion model (RIM) [7,8], rigid shell model (RSM) [9], valence shell model (VSM) [1], deformation dipole model (DDM) [10], bond bending force model (BBFM) [11,12], and bond charge model (BCM) [13]. These researchers have tried to interpret the phonon dispersion curves (PDCs) but none has

---

*Correspondence: jpdubebl@yahoo.com

succeeded in describing the PDCs and other results of ZnS very well. They have compared their theoretical results with their measured data but with only partial success.

The general descriptions of lattice dynamics having physical properties of ZBS semiconductors, i.e. the potentials that include the electrostatic interactions between the point charges and overlap repulsion between the nearest neighbors only, seem inadequate to take relativistic account of the crystal interactions in view of the phenomena of logical model calculations [7–16] and quantum mechanics [17,18]. Furthermore, the effects of long-range (LR) three body interactions (TBI), short-range (SR) interactions, and van der Waals (VDW) attraction are significant in partially ionic and covalent crystals [19]. Although VDW interactions (VDWI) have much effective force, Singh and Singh [20] used only three body force shell model (TSM) formulations for ZnS, ZnSe, and ZnTe without inclusion of VDWI. As far as the calculations on third order elastic constants (TOEC) and pressure derivatives of second order elastic constants (SOEC) are concerned, Sharma and Verma [21] have reformulated the expressions derived by Garg et al. [22]. They have derived the correct expressions for TOEC and pressure derivatives of SOEC for ZBS crystals. Various researchers [23–27] used their correct expressions for calculating the anharmonic elastic properties for NaCl, CsCl, and ZBS of solids. Therefore, we used the expressions of Sharma and Verma [21] as such for our computations.

The above information encouraged us to include (i) the effect of VDWI and (ii) TBI in the framework of RSM where short-range interactions are effective up to the second neighbors. Our new model thus developed is known as a van der Waals three body force rigid shell model (VTRSM). It has 14 parameters, i.e. four TBI parameters b, ρ, $f(r_0)$, r_0 $f'(r_0)$; six nearest and the next nearest neighbor short-range repulsive interaction parameters A_{12}, B_{12}, A_{11}, B_{11}, A_{22}, B_{22}; two distortion polarizabilities of negative and positive ions d_1, d_2; and two shell charges of the negative and positive ions Y_1, Y_2 respectively. They can be deduced with the help of measured values of elastic constants, dielectric constants, electronic polarizabilities and VDW coupling coefficients. This model has been applied to study the lattice dynamics of zinc chalcogenides (ZnS, ZnSe, ZnTe). In this paper, we report the study of phonon dispersion curves, Debye temperature variation, combined density of states (CDS), third order elastic constants, and pressure derivatives of SOEC. The formalism of our model is presented in the next section in detail.

2. Theoretical framework of the present model

We have developed a model that includes the effect of VDWI and TBI in the framework of a RSM where short-range interactions are effective up to the second neighbors and known as a VTRSM.

2.1. Secular equations

For ZBS crystals, the cohesive energy for a particular lattice separation (r) is expressed as

$$\Phi(r) = \Phi_{LR}(r) + \Phi_{SR}(r), \tag{1}$$

where the first term $\Phi_{LR}(r)$ represents the long-range Coulomb and TBI energies expressed by

$$\Phi_{LR}(r) = -\sum_{\substack{ij \\ i \neq j \neq k}} \frac{Z_i Z_j e^2}{r_{ij}} \left\{ 1 + \sum_k f(r_{ik}) \right\} = -\frac{\alpha_M Z^2 e^2}{r} \left\{ 1 + \frac{4}{Z} f(r) \right\}, \tag{2}$$

243

where Z_i is the ionic charge parameter of the ith ion, r_{ij} is separation between the ith and jth ion, f(r_{ik}) is the three body force parameter dependent on nearest-neighbor separation r_{ik} and is a measure of ion size difference [19], and α_M is the Madelung constant (=1.63805 for ZBS).

The second term in Eq. (1) is short-range energy contributions from overlap repulsion and VDWI expressed as [28]

$$\Phi_{SR}(r) = Nb \sum_{i,j=1}^{2} \beta_{ij} exp \left[\frac{r_i + r_j - r_{ij}}{\rho} \right] - \sum_{ij} \frac{C_{ij}}{r_{ij}^6} - \sum_{ij} \frac{d_{ij}}{r_{ij}^8}, \tag{3}$$

where N is the Avogadro's a number, b is the hardness parameter, and the first term is the Hafemeister and Flygare (HF) potential [29], used by Singh and coworkers [19,20,30]. The second term and third term represent the energy due to VDW coefficients for c_{ij} dipole–dipole (d–d) and d_{ij} dipole–quadrupole (d–q) interactions, respectively.

Using the crystal energy expression (1), the equations of motion of two cores and two shells can be written as

$$\omega^2 \underline{M} U = \left(\underline{R} + \underline{Z_m} \underline{C}' \underline{Z_m} \right) \underline{U} + \left(\underline{T} + \underline{Z_m} \underline{C}' \underline{Y_m} \right) W \tag{4}$$

$$O = \left(\underline{T}^T + \underline{Y_m} \underline{C}' \underline{Z_m} \right) \underline{U} + \left(\underline{S} + \underline{K} + \underline{Y_m} \underline{C}' \underline{Y_m} \right) \underline{W} \tag{5}$$

Here $\underline{U}$ and $\underline{W}$ are vectors describing the ionic displacements and deformations, respectively. $\underline{Z_m}$ and $\underline{Y_m}$ are diagonal matrices of modified ionic charges and shell charges, respectively; $\underline{M}$ is the mass of the core; $\underline{T}$ and $\underline{R}$ are repulsive Coulombian matrices, respectively; $\underline{C}'$ and $\underline{Y_m}$ are long-range interaction matrices that include Coulombian and TBI, respectively; $\underline{S}$ and $\underline{K}$ are core–shell and shell–shell repulsive interaction matrices, respectively, and $\underline{T}^T$ is the transpose of matrix $\underline{T}$. The elements of matrix $\underline{Z_m}$ consist of the parameter Z_m giving the modified ionic charge.

$$Z_m = \pm Z \sqrt{1 + \left(\frac{8}{Z} \right) f(r_0)} \tag{6}$$

The elimination of $\underline{W}$ from Eqs. (4) and (5) leads to the secular determinant

$$|\underline{D}(\vec{q}) - \omega^2 \underline{M} \underline{I}| = 0 \tag{7}$$

for the frequency determination. Here $\underline{D}$ (q) is the (6 × 6) dynamical matrix given by

$$\underline{D}(\vec{q}) = \left(\underline{R}' + \underline{Z_m} \underline{C}' \underline{Z_m} \right) - \left(\underline{T} + \underline{Z_m} \underline{C}' \underline{Y_m} \right) \times \left(\underline{S} + \underline{K} + \underline{Y_m} \underline{C}' \underline{Y_m} \right)^{-1} \left(\underline{T}^T + \underline{Y_m} \underline{C}' \underline{Z_m} \right) \tag{8}$$

The numbers of adjustable parameters were largely reduced by considering all the short-range interactions to act only through the shells.

2.2. Vibrational properties of ZBS

By solving the secular equation (4) along the [q00] direction and subjecting the short- and long-range coupling coefficients to the long-wavelength limit $\vec{q} \to 0$, two distinct optical vibration frequencies are obtained as

$$\left(\mu \omega_L^2 \right)_{q=0} = R_0' + \frac{(Z'e)^2}{v f_L} \frac{8\pi}{3} \left(Z_m^2 + 4Zr_0 f'(r_0) \right) \tag{9}$$

$$\left(\mu\omega_T^2\right)_{q=0} = R_0' - \frac{\left(Z'e\right)^2}{v f_T} \frac{4\pi}{3} Z_m^2, \tag{10}$$

where the abbreviations stand for

$$R_0' = R_0 - e^2 \left(\frac{d_1^2}{\alpha_1} + \frac{d_2^2}{\alpha_2}\right); R_0 = \frac{e^2}{v}\left[4\frac{A+2B}{3}\right]; Z' = Z_m + d_1 - d_2 \tag{11}$$

$$f_L = 1 + \left(\frac{\alpha_1+\alpha_2}{v}\right)\frac{8\pi}{3}\left(Z_m^2 + 4Z r_0 f'(r_0)\right) \tag{12}$$

$$f_T = 1 - \left(\frac{\alpha_1+\alpha_2}{v}\right)\frac{4\pi}{3} \tag{13}$$

and

$$\alpha = \alpha_1 + \alpha_2 \tag{14}$$

And $v = 3.08 r_0^3$ for ZBS (volume of the unit cell).

3. Debye temperature variation

The specific heat at constant volume C_v at temperature T is expressed as

$$C_v = 3Nk_B \frac{\int_0^{\nu_m}\left\{\left(\frac{h\nu}{k_BT}\right)^2 e^{h\nu/k_BT}\right\}G(\nu)d\nu}{\int_0^{\nu_m}G(\nu)d\nu} / \left(e^{h\nu/k_BT}-1\right)^2, \tag{15}$$

where ν_m is the maximum frequency, N is the Avogadro's a number, h is the Planck's constant, and k_B is the Boltzmann's constant. Eq. (15) can be written as a suitable form for a computational purpose as

$$C_v = 3Nk_B \frac{\sum_\nu \left\{E\left(x\right)\right\}G\left(\nu\right)d\nu}{\sum_\nu G(\nu)d\nu}, \tag{16}$$

where E(x) is the Einstein function, defined by

$$E\left(x\right) = x^2 \frac{\exp(x)}{\left(\exp\left(x\right)-1\right)^2}, \tag{17}$$

where $x = \left\{\left(\frac{h\nu}{k_BT}\right)^2 e^{\frac{h\nu}{k_BT}}\right\}$

Moreover,

$$\sum_\nu G(\nu)d\nu = \text{Total number of frequencies considered.}$$
$$= 6000 \, for \, ZBS.$$

Hence, Eq. (16) can be written for ZBS type crystals as

$$C_v = \frac{3Nk_B}{6000}\sum_\nu E\left(x\right)G\left(\nu\right)d\nu \tag{18}$$

The contribution of each interval to the specific heat is obtained by multiplying an Einstein function corresponding to the mid-point of each interval (say 0.1 THz) by its statistical weight. The statistical weight of the interval is obtained from the number of frequencies lying in that interval. The contributions of all such intervals when summed up give $\sum_{\nu} E(x) G(\nu) d\nu$. The specific heat C_v is then calculated by expression (18).

4. Second and third order elastic constant

Proceeding with the use of the three body crystal potential given by Eq. (1), Sharma and Verma [21] derived the expressions for the second order elastic constants and used by Singh and Singh [20] for ZBS crystals. We report them here as their corrected expressions.

The expressions for second order elastic constants (SOEC) are

$$C_{11} = L\left[0.2477Z_m^2 + \frac{1}{3}(A_1 + 2B_1) + \frac{1}{2}(A_2 + B_2) + 5.8243Zaf'(r_0)\right] \tag{19}$$

$$C_{12} = L\left[-2.6458Z_m^2 + \frac{1}{3}(A_1 - 4B_1) + \frac{1}{4}(A_2 - 5B_2) + 5.8243Zaf'(r_0)\right] \tag{20}$$

$$C_{44} = L\left[-0.123Z_m^2 + \frac{1}{3}(A_1 + 2B_1) + \frac{1}{4}(A_2 + 3B_2) - \frac{1}{3}\nabla(-7.539122Z_m^2) + A_1 - B_1\right], \tag{21}$$

where $A_1 = A_{12}$, $B_1 = B_{12}$, $A_2 = A_{11} + A_{22}$, $B_2 = B_{11} + B_{22}$, $C_1 = \frac{A_{12}^2}{B_{12}}$, and $C_2 = \frac{A_2^2}{B_2}$

and the expressions for third order elastic constants (TOEC) are

$$C_{111} = L\left[0.5184Z_m^2 + \frac{1}{9}(C_1 - 6B_1 - 3A_1) + \frac{1}{4}(C_2 - B_2 - 3A_2) - 2(B_1 + B_2) - 9.9326Zaf'(r_0) + 2.5220Za^2f''(r_0)\right] \tag{22}$$

$$C_{112} = L\left[0.3828Z_m^2 + \frac{1}{9}(C_1 + 3B_1 - 3A_1) + \frac{1}{8}(C_2 + 3B_2 - 3A_2) - 11.642Zaf'(r_0) + 2.5220Za^2f''(r_0)\right] \tag{23}$$

$$C_{113} = L\left[6.1585Z_m^2 + \frac{1}{9}(C_1 + 3B_1 - 3A_1) - 12.5060Zaf'(r_0) + 2.5220Za^2f''(r_0)\right] \tag{24}$$

$$
\begin{aligned}
C_{144} = L\Bigg[& 6.1585Z_m^2 + \frac{1}{9}(C_1 + 3B_1 - 3A_1) - 4.1681Zaf'(r_0) + 0.8407Za^2f''(r_0) + \\
& + \nabla\left\{-3.3507Z_m^2 - \frac{2}{9}C_1 + 13.5486Zaf'(r_0) - 1.681Za^2f''(r_0)\right\} \\
& + \nabla^2\left\{-1.5637Z_m^2 + \frac{2}{3}(A_1 - B_1) + \frac{1}{9}C_1 - 5.3138Zaf'(r_0) + 2.9350Za^2f''(r_0)\right\}\Bigg]
\end{aligned} \tag{25}
$$

$$
\begin{aligned}
C_{166} = L\Bigg[& -2.1392Z_m^2 + \frac{1}{9}(C_1 - 6B_1 - 3A_1) + \frac{1}{8}(C_2 - 5B_2 - 3A_2) - (B_1 + B_2) - 4.1681Zaf'(r_0) \\
& + 0.8407Za^2f''(r_0) + \nabla\left\{-8.3768Z_m^2 + \frac{2}{3}(A_1 - B_1) - \frac{2}{9}C_1 + 13.5486Zaf'(r_0) - 1.681Za^2f''(r_0)\right\} \\
& + \nabla^2\left\{2.3527Z_m^2 + \frac{1}{9}C_1 - 5.3138Zaf'(r_0) + 2.9350Za^2f''(r_0)\right\}\Bigg]
\end{aligned} \tag{26}
$$

$$C_{456} = L\left[4.897Z_m^2 + \frac{1}{9}\left(C_1 - 6B_1 - 3A_1\right) - B_2 + \nabla\left\{-5.0261Z_m^2 - \frac{1}{9}C_1\right\} + \nabla^2\left\{7.0580Z_m^2 + \frac{C_1}{3}\right\}\right.$$

$$\left. + \nabla^3\left\{-4.8008Z_m^2 + \frac{1}{3}\left(A_1 - B_1\right) - \frac{1}{9}C_1\right\}\right], \tag{27}$$

where Z_m is the modified ionic charge defined earlier by $L = e^2/4a^4$ and

$$\nabla = \left[\frac{-7.53912Z\left(Z + 8f\left(r_0\right)\right) + \left(A_1 - B_1\right)}{-3.141Z\left(Z + 8f\left(r_0\right)\right) + \left(A_1 + 2B_1\right) + 21.765Zaf'\left(r_0\right)}\right] \tag{28}$$

The values of Ai, Bi, and Ci are defined by Sharma and Verma [21].

5. Computations

The model parameters (b, ρ, and f(r_0)) were determined by using the expressions (19–21) and the equilibrium condition $\left(\frac{d\Phi(r)}{dr}\right)_{r_0 = a\frac{\sqrt{3}}{2}} = 0$, with the inclusion of the VDWI [Eq. (3)]. The values of the input data of Berlin Court et al. [31], Jai Shankar et al. [32] and Kunc et al. [33] and the model parameters are shown in Table 1. The values of A_i, B_i, and C_i were calculated from the knowledge of b and ρ and the values of various order of derivatives are f(r_0) (like f $'(r_0)$, $f''(r_0)$, $f'''(r_0)$) were obtained by using functional form $f(r_0) = f_0 e^{-r/\rho}$ as used by Singh and Singh [20]. The values of VDW coefficients used in the present study were determined using the Slater–Kirkwood variation (SKV) method [34] and the Lee [2] approach as suggested by Singh and Singh [20]. Thus our model parameters are b, ρ, f(r_0), r_0f $'(r_0)$, A_{12}, A_{11}, A_{22}, B_{12}, B_{11}, B_{22}, d_1, d_2, Y_1 and Y_2. These values of the VDW coefficients are shown in Table 2. Our model parameters of VTRSM were used to compute the phonon spectra for ZnS for the allowed 48 nonequivalent wave vectors in the first Brillouin zone. The frequencies along the symmetry directions were plotted against the wave vector to obtain the PDCs. These curves were compared with those measured by means of the coherent inelastic neutron scattering technique [1] in Figure 1 along with the DDM calculations of Kunc et al. [10]. Since the neutron scattering experiments provide us with very few data for the symmetry directions, we also computed the CDS and the Debye temperature variation for the complete description of the frequencies for the Brillouin zone.

The complete phonon spectra were used to compute the CDS and N($\nu_j + \nu_{j'}$) corresponding to the sum modes ($\nu_j + \nu_{j'}$) following the procedure of Smart et al. [35]. A histogram between N($\nu_j + \nu_{j'}$) and ($\nu_j + \nu_{j'}$) was plotted and smoothed out as shown in Figure 2. These curves show well defined peaks that correspond to two-phonon Raman scattering and IR absorption spectra. These CDS peaks were compared with the assignments calculated and shown in Table 3. The Debye temperature variation for ZnS measured by Martin [3] and Clusius and Hartech [4] and those calculated by us using VTRSM are compared in Figure 3. The calculated values of TOEC using Eqs. (22)–(27) were compared with calculated values of Anil et al. [36] and are shown in Table 4. The pressure derivatives of SOEC were also calculated and are compared with those calculated by Anil et al. [36] and Dinesh et al. [37] and measured by Madelung et al. [38] in Table 5. The Cauchy's discrepancy of TOEC was also calculated and is shown in Table 6.

Table 1. Input data and model parameters for ZnS [C_{ij} and B (in 10^{11} dyne/cm^2), ν (in THz), r_0 (in 10^{-8} cm), α_i (in 10^{-24} cm^3), b (in 10^{-12} erg), ρ (in 10^{-8} cm)].

Input data		Model parameters	
Properties	Values	Parameters	Values
C_{11}	10.46^a	b	1.8000
C_{12}	6.53^a	ρ	0.4850
C_{44}	4.61^a	$f(r_0)$	−0.0274
B	7.50^a	$r_0 f\,'(r_0)$	0.1322
r_0	2.34^a	A_{12}	19.7684
$\nu_{LO}(\Gamma)$	10.44^b	B_{12}	−6.3279
$\nu_{TO}(\Gamma)$	8.30^b	A_{11}	95.9119
$\nu_{LO}(L)$	10.41*	B_{11}	−20.5278
$\nu_{TO}(L)$	8.51*	A_{22}	−2.4330
$\nu_{LA}(L)$	4.24^b	B_{22}	−7.1774
$\nu_{TA}(L)$	1.68^b	d_1	0.3515
α_1	1.01^c	d_2	2.7619
α_2	5.12^c	Y_1	−2.0428
ε_0	8.54^d	Y_2	−1.3179

* Extrapolated values from [1].
^{a}-(Berlin Court et al. [31]); ^{b}- (Vagelatos et al. [1]); ^{c}- (Shankar et al. [32]); ^{d}- (Kunc et al. [33]).
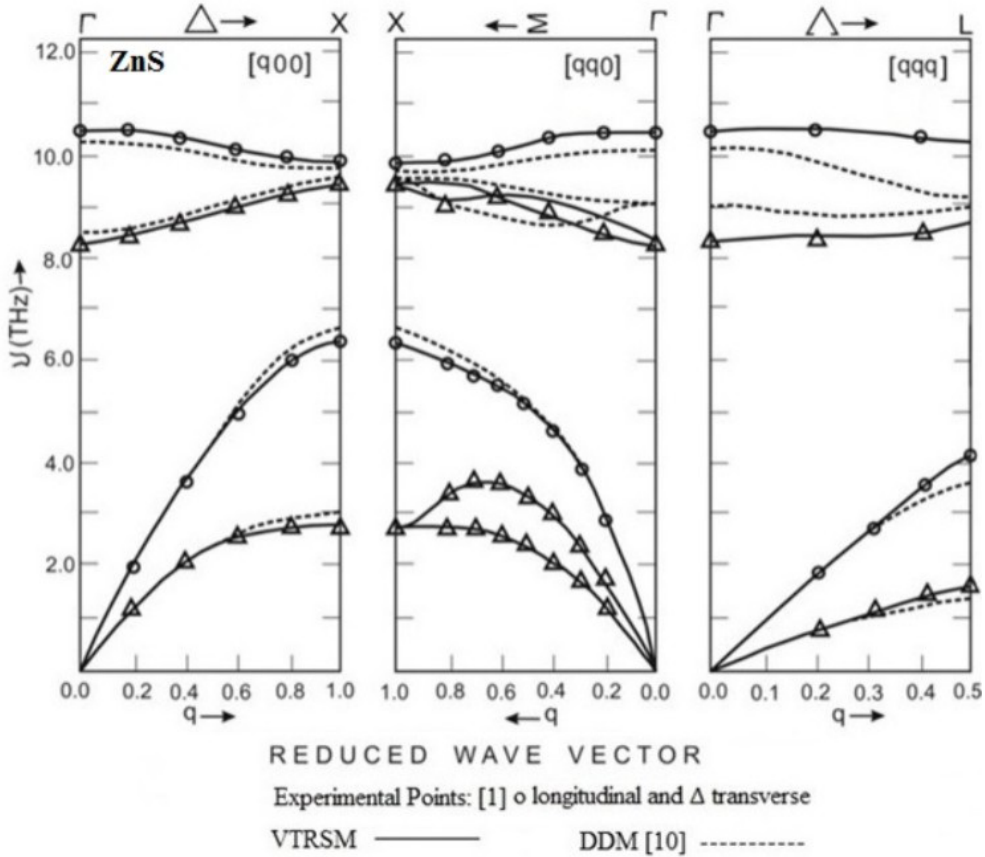

Figure 1. Phonon dispersion curves for ZnS at room temperature.
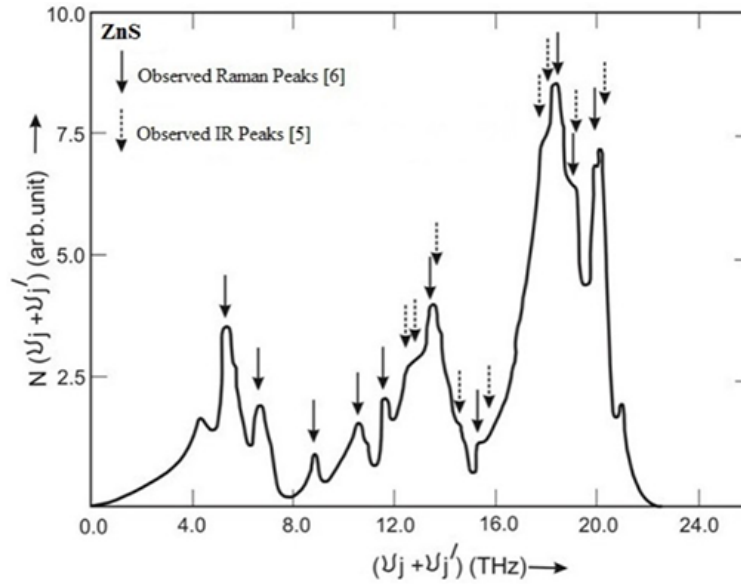
Figure 2. Combined density of states curve for ZnS.
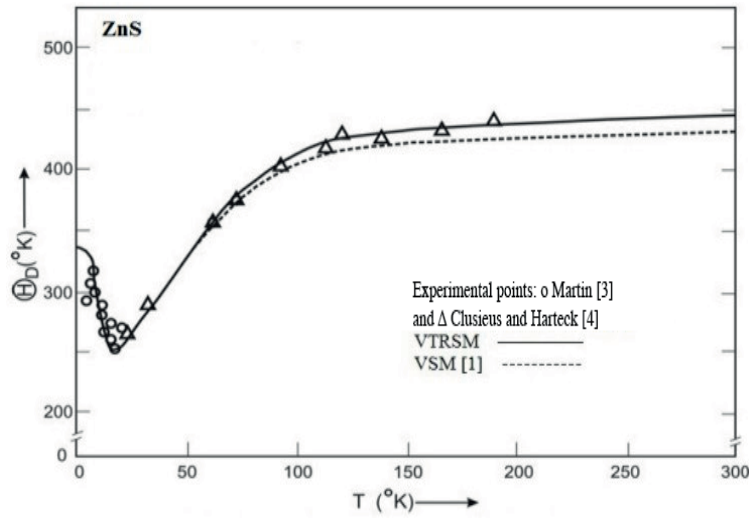
Figure 3. Debye characteristic temperatures $\Theta_D(^\circ K)$ as a function of temperature T for ZnS.

Table 2. Van der Waals interaction coefficients for ZnS (C_{ij} and C in units of 10^{-60} erg cm^6 and d_{ij} and D in units of 10^{-76} erg cm^8).

Parameters	Numerical values
C_{+-}	165
C_{++}	60
C_{--}	580
d_{+-}	111
d_{++}	19
d_{--}	498
C	956
D	508

Table 3. Assignments for the observed peak positions in combined density of states in terms of selected phonon frequencies at Γ, X, and L critical points for ZnS.

CDS peaks (cm^{-1})	Raman active			Infrared active		
	Observed	Present study		Observed IR	Present study	
	Ramadan peaks (cm^{-1}) [6]	Values (cm^{-1})	Assignments	peaks (cm^{-1}) [5]	Values (cm^{-1})	Assignments
142	....	....	....	....	....	....
177	176	180	2TA(X)	....	....	....
220	219	217	TO–TA (Δ)	....	....	....
293	295	302	LA+TA(X)	....	....	....
353	352	....	....	....	....	....
387	386	383	TO+TA (Δ)	....	383	TO+TA (Δ)
420	....	420	LO+TA (Δ)	415	420	LO+TA (Δ)
....	....	....	....	431	432	TO+LA (L)
450	448	467	TO+LA (Δ)	455	467	TO+LA (Δ)
....	....	....	....	491	482	LO+LA (L)
510	511	504	LO+LA (Δ)	526	504	LO+LA (Δ)
....	....	584	2TO(L)	593	....	....
600	....	600	2TO(Δ)	605	600	2TO(Δ)
613	612	....	....	....	....	....
633	636	634	2TO(X)	....	....	....
....	....	634	LO+TO (L)	....	....	....
....	....	637	LO+TO(Δ)	642	637	LO+TO(Δ)
660	665	656	2LO(X)	....	....	....
670	....	674	2LO(Δ)	677	674	2LO(Δ)
....	....	684	2LO(L)	733	....	....
700	....	696	2LO(Γ)	....	....	....
....	....	....	....	823	....	....

Table 4. Third order elastic constants (in the unit of 10^{11} dyne/cm^2) for ZnS.

Property	Present study	Other theoretical results [36]
C_{111}	–95.51	–60.95
C_{112}	–115.15	–30.71
C_{123}	–1.87	–47.20
C_{144}	1.02	–40.00
C_{166}	–29.17	–30.00
C_{456}	35.65	–98.90

Table 5. Values of pressure derivatives of SOEC (dimensionless) for ZnS.

Properties	Values			
	Present Study	Other [36]	Other [37]	Experimental [38]
dK'/dP	3.17	5.12	....	4.90
dS'/dP	–0.56	–0.50	....	....
dC'_{44}/dP	0.09	1.14	1.6	....

Table 6. Values of Cauchy discrepancy of TOEC (in the unit 10^{11} dyne cm^{-2}) for ZnS.

Properties	Values
C_{112}–C_{166}	–66.09
C_{123}–C_{456}	27.87
C_{144}–C_{456}	15.50
C_{123}–C_{144}	–8.72

6. Results and discussion

6.1. Phonon dispersion curves

From Figure 1, our phonon dispersion curves for ZnS agree well with measured data reported by Vagelatos et al. [1] at room temperature. It is evident from PDCs that our predictions using the present model (VTRSM) are better than those by using DDM [10]. Our model successfully explained the dispersion of phonons along the three symmetry directions. From Figure 1 and Table 7, it is clear that there are deviations of 1.01% along LO(X), 1.17% along TO(X), 4.74% along LA(X), 11.15% along TA(X), 13.44% along LA(L), and 16.08% along TA(L). From DDM, deviations are 11.52% along TA(X), 13.91% along LA(L) and 16.67% along TA(L) while from VTRSM 0.37% along TA(X), 0.47% along LA(L) and 0.50% along TA(L). From Table 7 it is clear that VTRSM has very small deviation from the experimental data. Our model, VTRSM, has 16.08% improvement over DDM due to the inclusion of TBI and VDWI coefficients. Therefore, our VTRSM has better agreement with the experimental data over DDM [10].

Table 7. Comparison of frequencies from various sources (X and L points) for ZnS.

Points	Branches (THz)	Expt. [1]	DDM [10]			Present Study			% Improvement (a ~ b) over DDM
			Value	(±) Deviation	% (a)	Value	(±) Deviation	% (b)	
X (100)	LO	9.90	9.75	0.15	1.51	9.85	0.05	0.50	1.01
	TO	9.47	9.60	0.14	1.48	9.50	0.03	0.31	1.17
	LA	6.34	6.65	0.31	4.89	6.35	0.01	0.15	4.74
	TA	2.69	3.00	0.31	11.52	2.70	0.01	0.37	11.15
L (.5.5.5)	LO	....	9.20	....	....	10.25	....	....	....
	TO	....	9.00	....	....	8.75	....	....	....
	LA	4.24	3.65	0.59	13.91	4.22	0.02	0.47	13.44
	TA	1.68	1.40	0.28	16.67	1.67	0.01	0.50	16.08

6.2. Combined density of states

The present model is capable of predicting the two phonon Raman/IR spectra [5,6]. The results of these investigations for CDS peaks are presented in Figure 2. The theoretical peaks are in good agreement with both observed Raman/IR spectra for ZnS. The assignments made by the critical point analysis are shown in Table 3. The interpretation of Raman/IR spectra achieved from both the CDS approach and critical point analysis is quite satisfactory. This shows that there is excellent agreement between the experimental data and our theoretical results.

6.3. Third order elastic constants (TOEC), pressure derivatives of second order elastic constants (SOEC), and values of Cauchy's discrepancy

Our calculations on TOEC are reported in Table 4. Since there are no measured data on TOEC of ZnS, no comparison could be made but our results were compared with the theoretical results of Anil et al. [36]. Further, pressure derivatives of SOEC for ZnS were also compared with the calculated results of Dinesh et al. [37] and measured data of Madelung et al. [38] as shown in Table 5. The results are in good agreement. Cauchy's discrepancy of TOEC was also calculated for ZnS and is shown in Table 6. It is hoped that our values on TOEC will be helpful to experimental workers in analyzing measured data in future.

6.4. Debye temperature variation

From Figure 3, our study shows better agreement with the measured data of Martin [3] and Clusius and Harteck [4] and the theoretical results reported by Vagelatos et al. [1] using VSM. To conclude, we can say that our model gives a better interpretation of the Debye temperature variation for ZnS.

7. Conclusion

The inclusion of VDWI with TBI influenced both the optical branches and the acoustic branches. Another striking feature of the present model is the excellent reproduction of almost all branches. Hence the prediction of PDC for ZnS using VTRSM may be considered more satisfactory than from the other models DDM [9,10] and BBFM [11,12]. The basic aim of the study of two phonon Raman/IR spectra is to correlate the neutron scattering and optical measured data of ZnS. In this paper, we systematically reported phonon dispersion curves, combined density of states, Debye temperature variation, and a part of harmonic and anharmonic properties of ZnS. On the basis of the overall discussion, it is concluded that our VTRSM is adequately capable of describing the crystal dynamics of zinc sulfide. This model may also be applied equally well to study the crystal dynamics of other compounds of this group (ZnSe and ZnTe).

Acknowledgments

References

[1] Vagelatos, N.; Wehe, D.; King, S. J. *J. Chem. Phys.* **1974**, *60*, 3613–3618.

[2] Lee, B. H. *J. Appl. Phys.* **1970**, *41*, 2988–2990.

[3] Martin, D. L. *Phil. Mag.* **1955**, *46*, 751–758.

[4] Clusius, K.; Harteck, P. *Z. Phys. Chem.* **1928**, *134*, 243–263.

[5] Deutsch, T.: in Proc. Int. Conf. Semiconductors, Exeter, Institute of Physics and Physical Society, London, 1962.

[6] Nilsen, W. G.: Proc. Int. Conf. Light Scattering Spectra of Solids, 1968.

[7] Vetelino, J. F.; Mitra, S. S. *Phys. Rev.* **1969**, *178*, 1349–1352.

[8] Talwar, D. N.; Vandevyver, M.; Kunc, K.; Zigone, M. *Phys. Rev. B* **1981**, *24*, 741–753.

[9] Kunc, K.; Nielsen, O. H. *Computer Phys. Commun.* **1979**, *17*, 413–422.

[10] Kunc, K.; Balkanski, M.; Nusimovici, M. A. *Phys. Rev. B* **1975**, *12*, 4346–4355.

[11] Kushwaha, M. S. *Phys. Rev. B* **1981**, *24*, 2115–2120.

[12] Kushwaha, M. S.; Kushwaha, S. S. *Canad. J. Phys.* **1980**, *58*, 351–358.

[13] Rajput, B. D.; Browne, D. A. *Phys. Rev. B* **1996**, *53*, 9052–9058.

[14] Yu, Y.; Zhou, J.; Han. H.; Zhang, C.; Cai, T.; Song, C.; Gao, T., *J. Alloys Compd.* **2009**, *471*, 492–497.

[15] Cardona, M.; Kremer, R. K.; Lauck, R.; Siegle, G.; Munoz, A.; Romero, A. H.; Schindler, A. *Phys. Rev. B* **2010**, *81*, 075207–075220.

[16] Wang, H. Y.; Cao, J.; Haung, X. Y.; Huang, J. M. *Cond. Matter Phys.* **2012**, *15*, 13705–13715.

[17] Lowdin, P. O. *Phil. Mag. Suppl.* **1956**, *5*, 1–15.

[18] Lundqvist, S. O. *Ark. Fys. Sweden* **1955**, *9*, 435–445.

[19] Singh, R. K. *Physics Reports* (Netherlands) **1982**, *85*, 259–401.

[20] Singh, R. K.; Singh, S. *Phys. Status Solidi (b)* **1987**, *140*, 407–413.

[21] Sharma, U. C.; Verma, M. P. *Phys. Status Solidi (b)* **1980**, *102*, 487–494.

[22] Garg, V. K.; Puri, D. S.; Verma, M. P. *Phys. Status Solidi (b)* **1978**, *87*, 401–407.

[23] Upadhyaya, K. S.; Pandey, A; Srivastava, D. M. *Chinese J. Phys.* **2006**, *44*, 127–136.

[24] Upadhyaya, K. S.; Upadhyay, G. K.; Yadav, M.; Singh, A. K. *J. Phys. Soc. Japan* **2001**, *70*, 723–728.

[25] Tiwari, S. K.; Pandey, L. K.; Shukla, L. J. Upadhyaya, K. S. *Phyica Scr.* **2009**, *80*, 1–6.

[26] Srivastava, U. C.; Upadhyaya, K. S. *Physical Rev. Res. Int.* **2011**, *1*, 16–28.

[27] Mishra, K. K.; Upadhyaya, K. S. *Int. Jour. Sci. Engg. Res.* **2012**, *3*, 1388–1398.

[28] Singh, R. K.; Khare, P. *J. Phys. Soc. Japan* **1982**, *51*, 141–146.

[29] Hafemeister, D. W.; Flygare. W. H. *J. Chem. Phys.* **1965**, *43*, 795–805.

[30] Singh, R. K.; Singh, R. D. *Phys. Status Solidi (b)* **1982**, *114*, 235–242.

[31] Berlin Court, D.; Jaffe, H.; Shiozawa, L. R. *Phys. Rev.* **1963**, *129*, 1009–1017.

[32] Shankar, J.; Sharma, J. C.; Sharma, O. P. *Ind. J. Pure Appl. Phys.* **1977**, *15*, 809–811.

[33] Kunc, K.; Balkanski, M.; Nusimovici, M. A. *Phys. Status Solidi (b)* **1975**, *72*, 249–260.

[34] Slater, J. C.; Kirkwood, J. G. *Phys. Rev.* **1931**, *37*, 682–697.

[35] Smart, C.; Wilkinson, G. R.; Karo, A. M.; Hardy, J. R. In *Lattice Dynamics*; Wallis, R. F. Ed. Pergamon Press: Oxford, UK, 1965.

[36] Anil, T. V.; Menon, C. S.; Kumar Krishna K. Shree; Chandran, K. P.; Jaya, *J. Phys., Chem. Sol.* **2004**, *65*, 1053–1057.

[37] Varshney, D.; Sharma, P.; Kaurav, N.; Singh, R. K. *Bull. Mat. Sci.* **2005**, *28*, 651–661.

[38] Madelung, O.; Schulz, M.; Weiss, H. *Physics of II-VI and I-VII Compounds Semimagnetic, Semiconductors*; Springer-Verlag: Berlin, Germany, 1982.